Electronic Supplementary Information (ESI)

Mechanochemical synthesis and application of mixed-metal copper-ruthenium HKUST-1 metal-organic frameworks in the electrocatalytic oxygen evolution reaction

Linda Sondermann,[a] Quentin Smith,[a,b] Till Strothmann,[a] Annette Vollrath,[a] Thi Hai Yen Beglau,[a] and Christoph Janiak *[a]

[a.] Institut für Anorganische Chemie und Strukturchemie, Heinrich-Heine-Universität Düsseldorf, 40204 Düsseldorf, Germany

[b.] Department of Chemistry, Virginia Polytechnic Institute and State University, Blacksburg, VA 24061, USA

* Correspondence: janiak@uni-duesseldorf.de (C.J.)

Email addresses: linda.sondermann@hhu.de, qsmith1713@vt.edu, till.strothmann@hhu.de, annette.vollrath@hhu.de, beglau@hhu.de

Brief HKUST-1 structure description

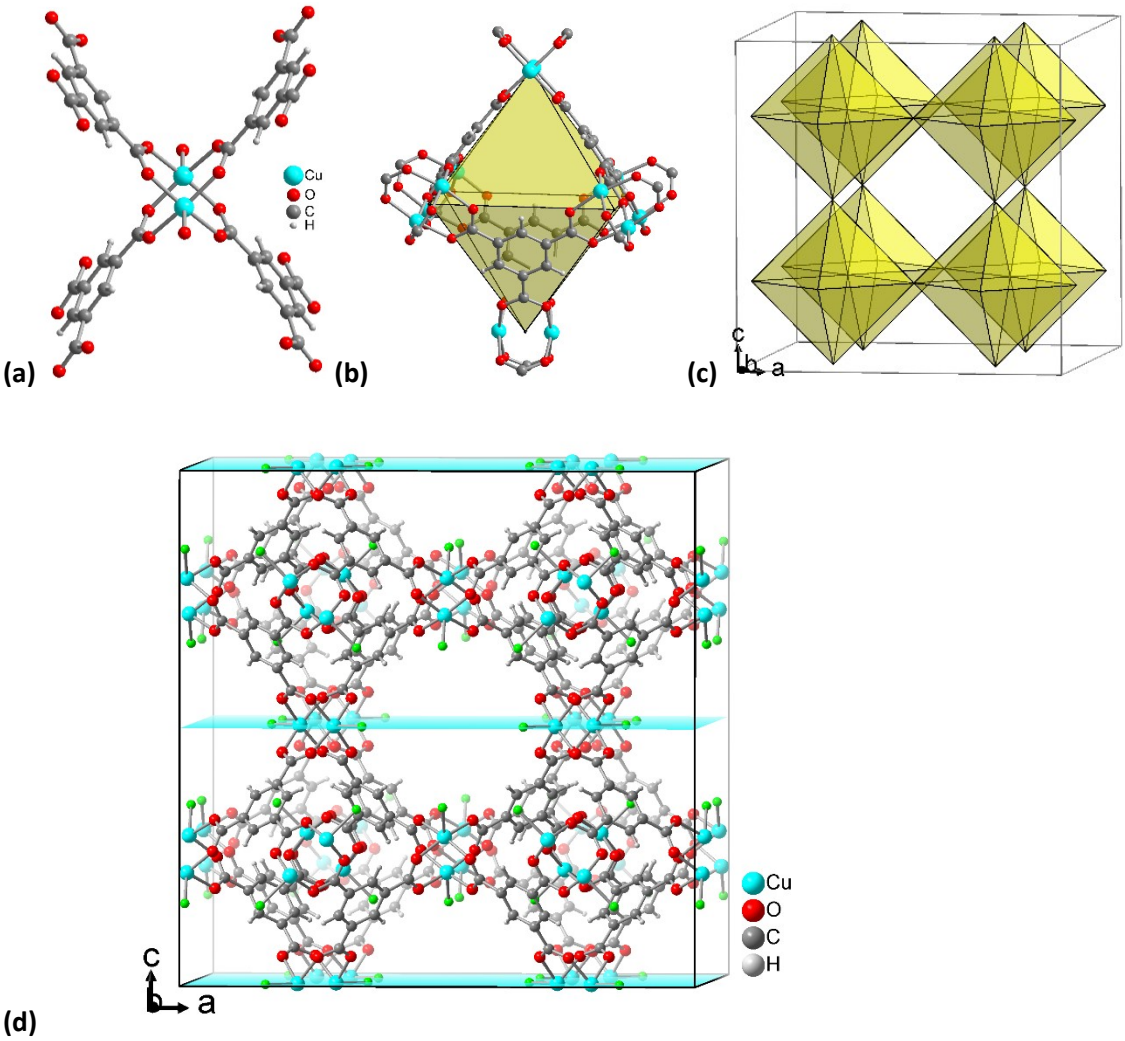

Fig. S1 (a) $\{Cu_2(btc)_4\}$ "paddle-wheel" unit in Cu-BTC (HKUST-1).
(b) The $\{Cu\}_2$ dumbbells sit at the corners of an octahedron. Four btc ligands span opposite four of the eight faces of the octahedron, forming octahedral side (A) cavities (5 Å) which are connected to the main channels by triangular windows (3.5 Å).
(c) These octahedra form a porous cubic 3D network via vertex linkage. Inside eight octahedra are larger cuboctahedral pores (11 Å, B and C cages depending on the position of the labile axial ligand), which are surrounded by eight octahedral faces and 12 paddle-wheel subunits. These cuboctahedral pores are connected through square-shaped windows (9 Å) giving channels along the *a*, *b*, and *c* axis. The specific surface area reaches ~1300-1500 m^2/g.
(d) The unit cell packing in HKUST-1 with the (002) lattice planes shown in cyan. In the cubic crystal system, the lattice planes (002) = (020) = (200) are equivalent to by the symmetry of the lattice. The possible aqua ligands on Cu are depicted in green for differentiation to the carboxylate O atoms.

Energy-dispersive X-ray spectroscopy (EDX) from scanning electron microscopy (SEM)

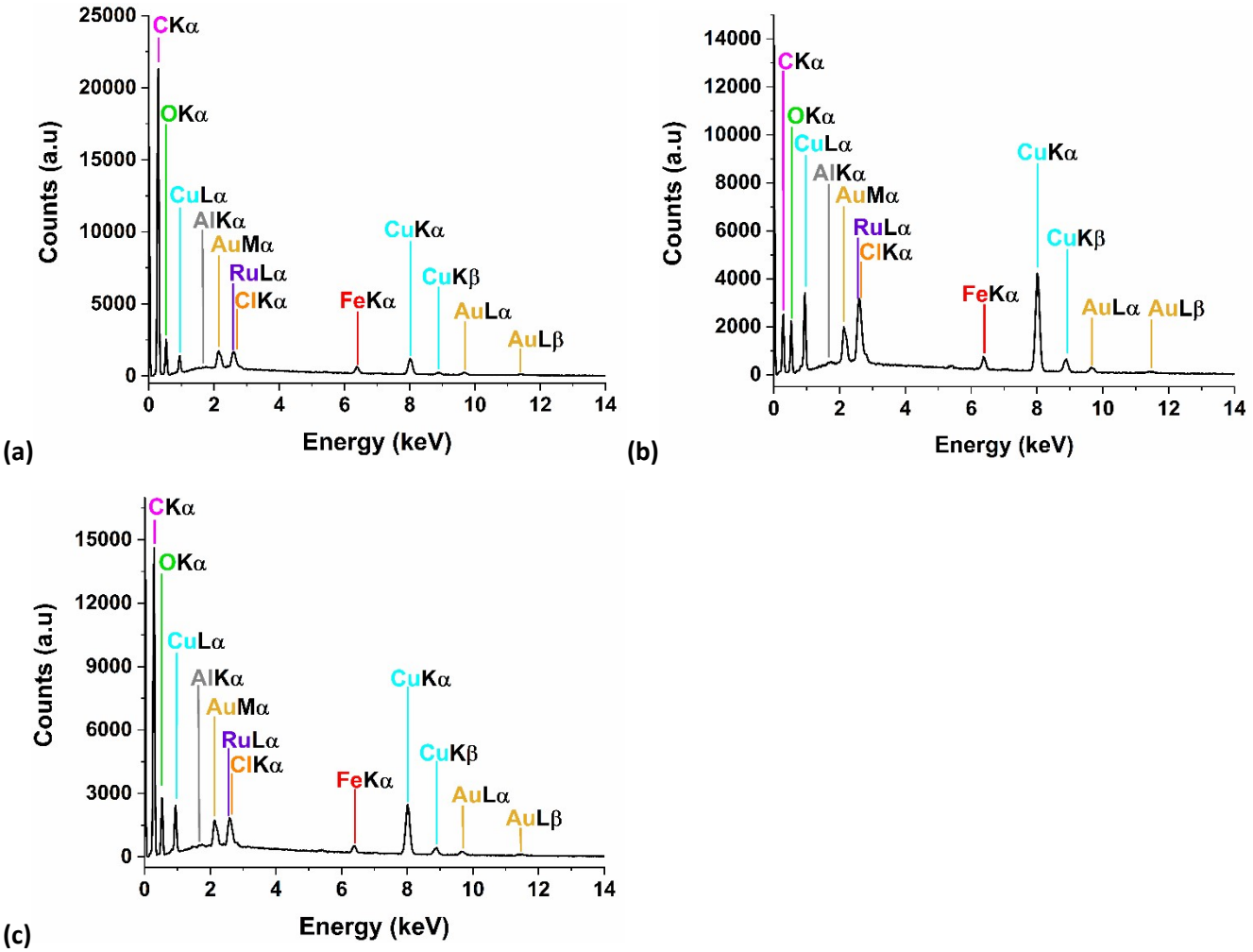

Fig. S2 SEM-EDX spectra of (a) Cu_6Ru-BTC, (b) Cu_7Ru-BTC and (c) Cu_{10}Ru-BTC. The Al and Au signals in the EDX spectra can be attributed to the Al sample holder and the sputtering of the sample with gold before the measurement.

Scanning electron microscopy (SEM)

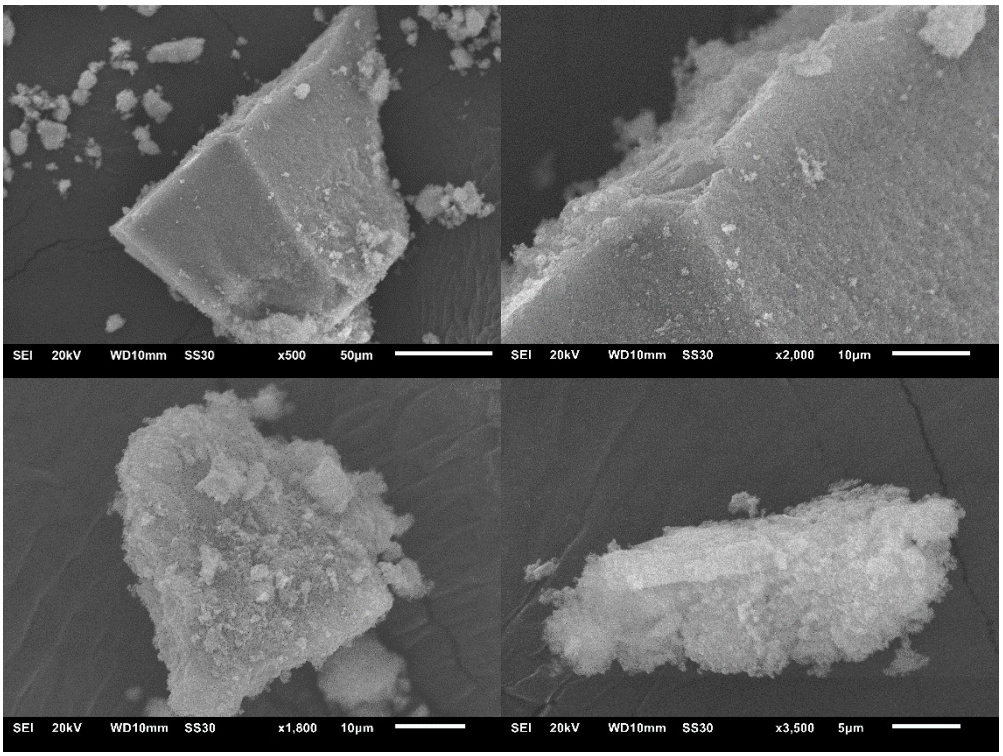

Fig. S3 Mechanochemically synthesized HKUST-1 SEM images.

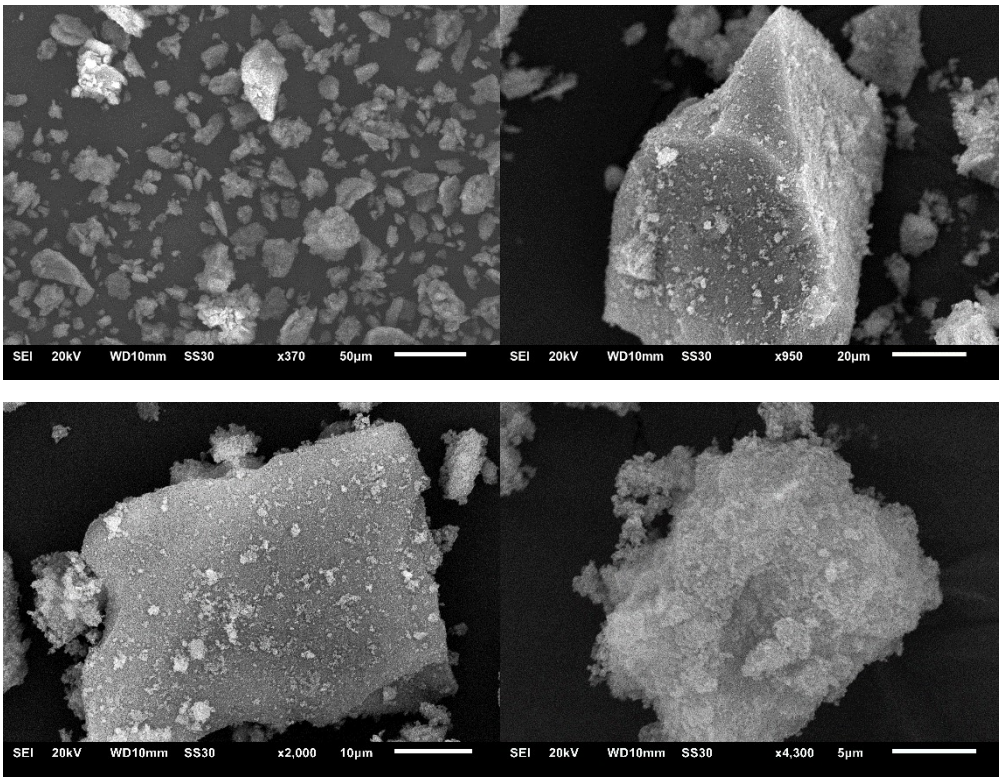

Fig. S4 Cu_6Ru-BTC SEM images.

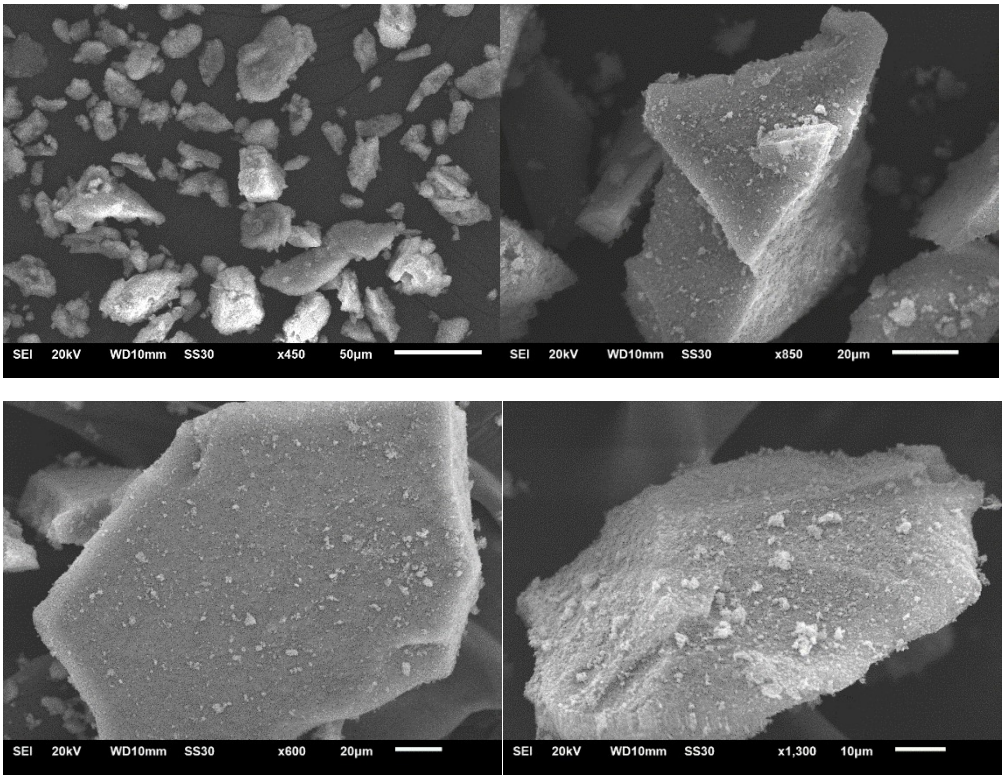

Fig. S5 Cu_7Ru SEM images.

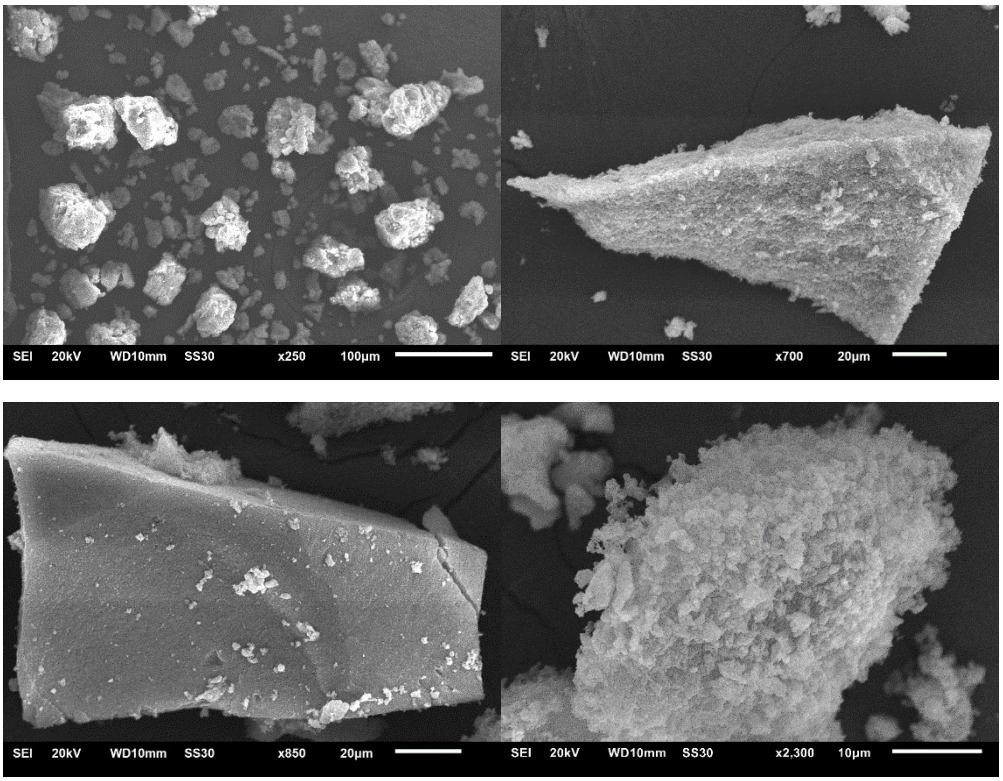

Fig. S6 $Cu_{10}Ru$ SEM images.

Transmission electron microscopy (TEM) images with EDX

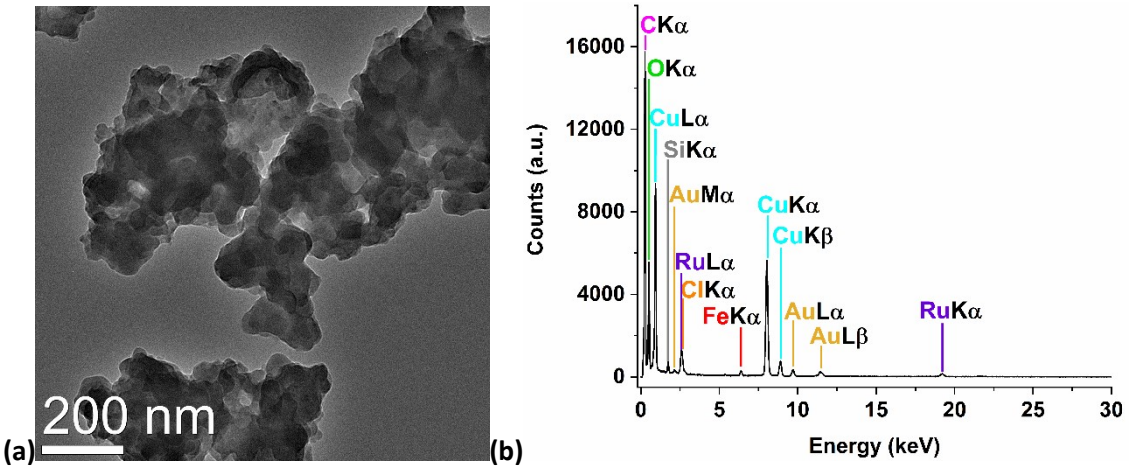

Fig. S7 (a) Transmission electron microscopy (TEM) image of Cu_6Ru-BTC, (b) TEM-EDX of Cu_6Ru-BTC.

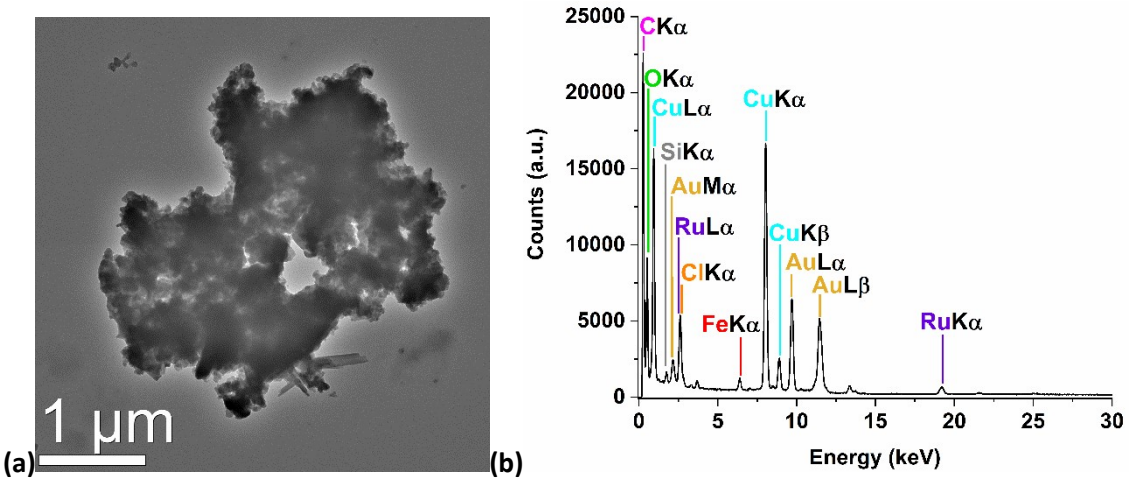

Fig. S8 (a) TEM image of Cu_8Ru-BTC, (b) TEM-EDX of Cu_8Ru-BTC.

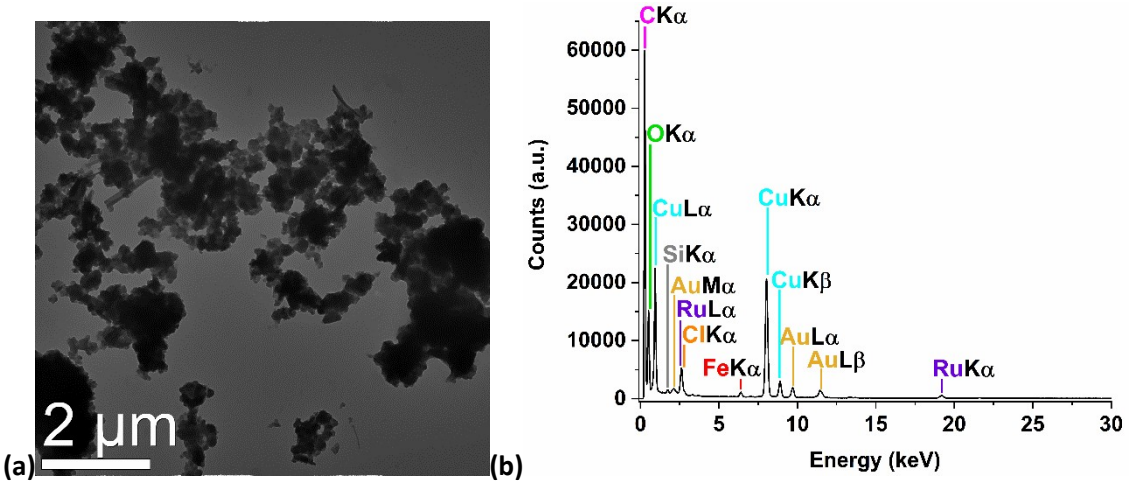

Fig. S9 (a) TEM image of $Cu_{10}Ru$-BTC, (b) TEM-EDX of $Cu_{10}Ru$-BTC.

Powder X-ray diffraction (PXRD)

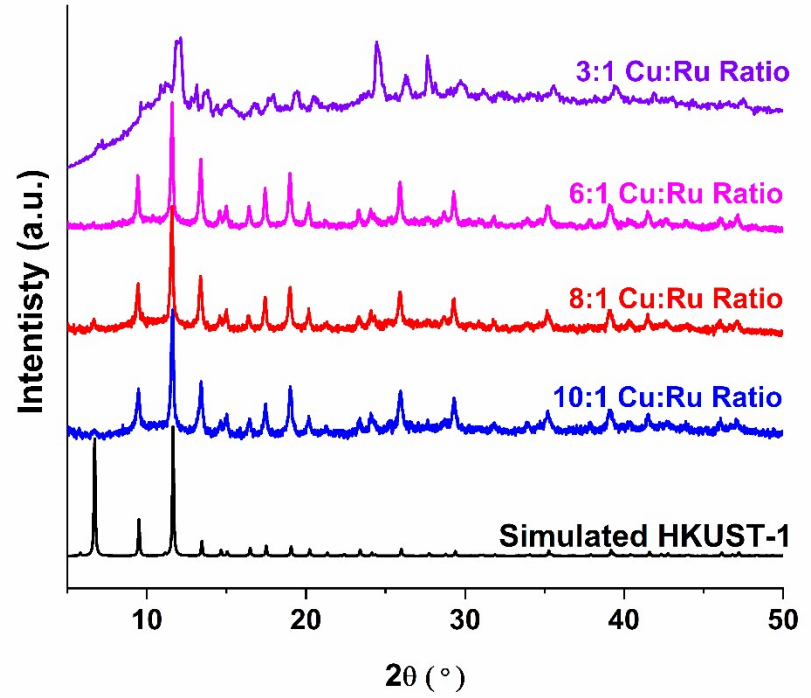

Fig. S10 PXRD patterns of Cu_6Ru-BTC (6:1 Cu:Ru), Cu_7Ru-BTC (8:1 Cu:Ru), $Cu_{10}Ru$-BTC (10:1 Cu:Ru), simulated HKUST-1 (CCDC no. 112954) and the attempted 3:1 Cu:Ru sample.

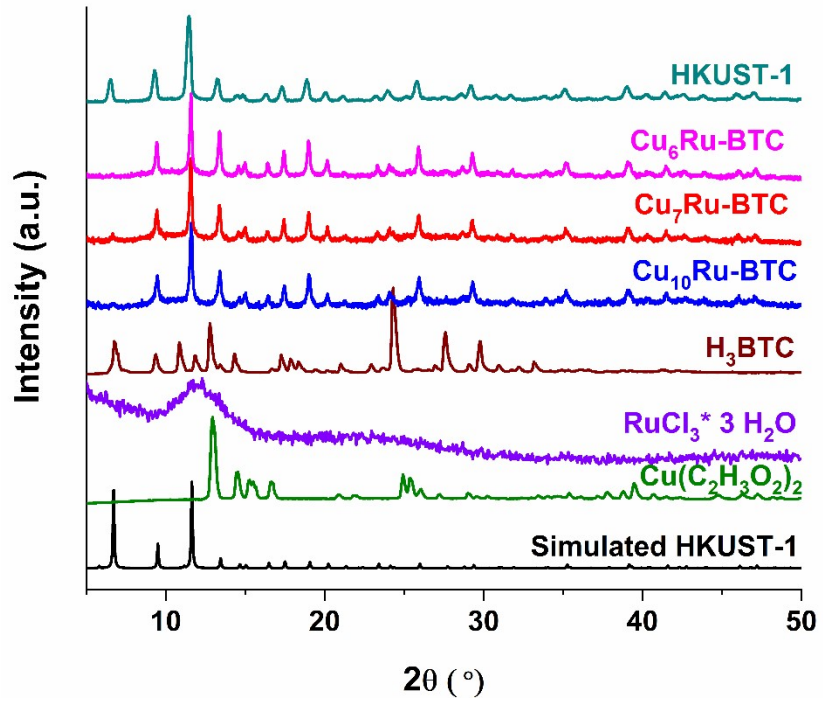

Fig. S11 PXRD patterns of Cu_6Ru-BTC, Cu_7Ru-BTC, $Cu_{10}Ru$-BTC, mechanochemically synthesized HKUST-1, simulated HKUST-1 (CCDC no. 112954) and their educts.

Thermogravimetric analysis (TGA)

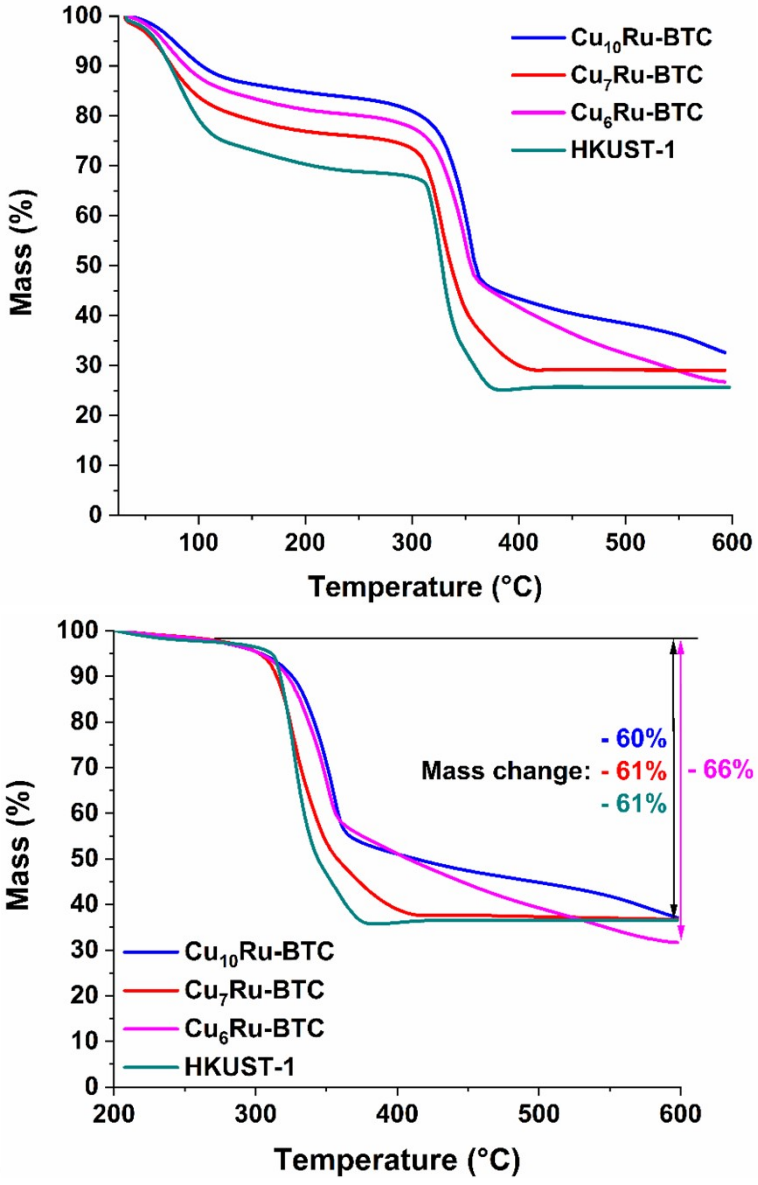

Fig. S12 (a) TGA data of Cu_6Ru-BTC, Cu_7Ru-BTC, Cu_{10}Ru-BTC and mechanochemically synthesized HKUST-1. For the TGA, the samples were used as-synthesized and had not been activated. (b) Rescaled TGA data of (a) by setting the value at 200 °C to 100%. A heating rate of 10 K/min under a N_2 atmosphere was used.

The residual mass of the TGA was slightly higher than the theoretical mass for Cu metal of 31.5 wt% and slightly higher for Cu_xRu, which is probably due to the formation of CuO in a mixture with Cu and Cu_2O (respectively Ru/RuO_x), from the Cu(Ru)-O bonds in the framework, which was also seen by Chen *et al.* even while measuring under high purity nitrogen atmosphere.[1] For simplicity we have only calculated with the formation of CuO. The expected theoretical residual mass of CuO for HKUST-1 would be 39.5 wt%. To correlate the mass loss of the linker to the residual metal oxide mass, the TGA is replotted by starting after the solvent loss at 200 °C with 100%. The values for the linker to the metal oxide mass loss are collected in Table S1. When the mass loss of the linker between ~280-600 °C is related to the residual mass (set as CuO), molar linker:metal ratios in the range of 1.8:3.2 to 2.0:2.7 are

obtained. The theoretical molar BTC:Cu ratio in HKUST-1 is 2:3, corresponding to 60.5 wt% BTC and 39.5 wt% CuO.

Table S1 TGA values for the linker mass loss and residual mass and the resulting linker (BTC) to metal (Cu) molar ratio.[a]

	BTC (wt%)	CuO (residual wt%)	molar linker to metal ratio
Cu_{10}Ru-BTC	60.1	39.9	1.83:3.17
Cu_7Ru-BTC	60.7	39.3	1.85:3.12
Cu_6Ru-BTC	65.7	34.3	2.00:2.72
HKUST-1	60.8	39.2	1.85:3.11
$[Cu_3(BTC)_2]$ calculated	60.5	39.5	2:3

[a] For the Cu_xRu-BTC samples, the values for HKUST-1 are used for comparison and the residual wt% was taken as CuO only. No individual % calculations to estimate the BTC loss and residual Cu/Ru-oxide content was done for simplicity. Also the probably formation of a mixture of Cu(Ru), Cu_2O and CuO (Ru-oxides) is not taken into account.

Elemental analysis

We analyzed the samples via CH elemental analysis and the results can be found in Table S2 below. As an example, the found values for HKUST-1 ($[Cu_3(BTC)_2]$) were 30.43% C and 3.34% H. This matches the mass% of C and H for, e.g., $[Cu_3(BTC)_2] \cdot 10\ H_2O$ 10 MeOH with 30.42% C and 3.29% H, which approximates the content of solvent molecules in this sample (Table S2†). Further, from the mass loss in the TGA up to 200 °C, the solvent content in the samples lies between 10-30 wt% which correlates with the approximations from CH analysis (Table S2†).

Table S2 CH elemental analysis of the MOF samples.[a]

	exp. values		calculated to estimate solvent content [b]			
	C (%)	H (%)	$[Cu_3(BTC)_2]$·xsolvent (wt% solvent)	C (%)	H (%)	wt% solvent from TGA (cf. Fig. S12a)
Cu_{10}Ru-BTC	29.14	3.62	$[Cu_3(BTC)_2] \cdot 8\ H_2O$ 0.5 MeOH (21)	29.04	2.97	9 (100 °C) 15 (200°C)
Cu_7Ru-BTC	31.54	3.04	$[Cu_3(BTC)_2] \cdot 5.5\ H_2O$ 1.5 MeOH (20)	31.14	2.49	16 (100 °C) 23 (200°C)
Cu_6Ru-BTC	32.37	3.13	$[Cu_3(BTC)_2] \cdot 5\ H_2O$ 3 MeOH (24)	31.88	2.43	12 (100 °C) 18 (200°C)
HKUST-1	30.43	3.34	$[Cu_3(BTC)_2] \cdot 8\ H_2O$ 5 MeOH (33)	30.38	3.00	21 (100 °C) 30 (200°C)
$[Cu_3(BTC)_2]$ calculated	35.74	1.00				

a Methanol (MeOH) was used in the mechanochemical synthesis and water (H_2O) can be due to crystal water from the educts, which were used in the mechanochemical synthesis, and adsorbed as moisture from the air. [b] In the % calculations to estimate the solvent content the Ru content or the exchange of 14 mol% (in Cu_6Ru) to 9 mol% (in Cu_{10}Ru) with the higher mass or Ru (101.07 g/mol) vs. Cu (63.55 g/mol) was neglected for simplicity.

Table S3 Cu and Ru analysis from AAS.

	Measured Cu (mg/L)	Calculated Cu (mg/L)[a]	Cu (mol/L)	Measured Ru (mg/L)	Calculated Ru (mg/L)[b]	Ru (mol/L)
$Cu_{10}Ru$-BTC	0.800	40.00	6.30×10^{-4}	5.601	6.220	6.20×10^{-5}
Cu_7Ru-BTC	0.767	38.35	6.04×10^{-4}	7.467	8.300	8.22×10^{-5}
Cu_6Ru-BTC	0.729	36.45	5.74×10^{-4}	8.162	9.070	8.98×10^{-6}

[a] In sample solution before 1:50 (v:v) dilution for the measurement; the Cu calibration curve was straight line going through the point of origin (0; 0). [b] In sample solution before 9:1 (v:v) dilution for the measurement of Ru, the dilution was brought about by the addition of 1 mL of a $LaCl_3 \times 7\ H_2O$ solution (c = 10 g/L in 10% HCl) added to 9 mL of the analysis solution; the Ru calibration curve was going through the point of origin (0; 0).

Infrared spectroscopy (IR)

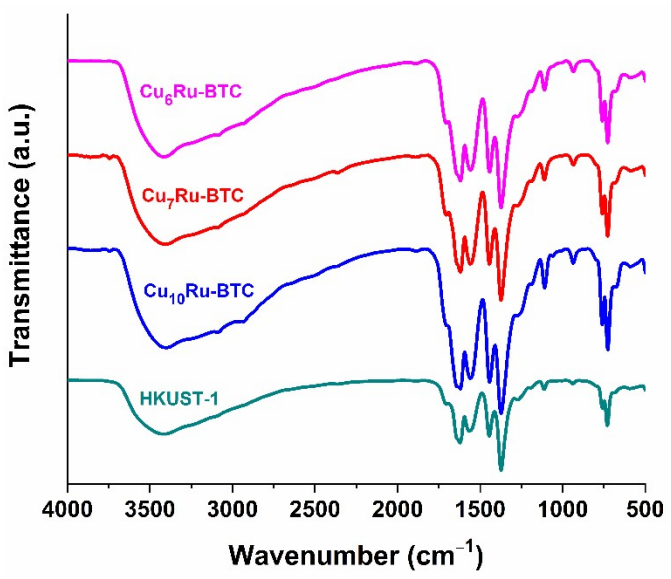

Fig. S13 FT-IR spectra for Cu_6Ru-BTC, Cu_7Ru-BTC, $Cu_{10}Ru$-BTC and mechanochemically synthesized HKUST-1.

Porosity related parameters derived from N_2-soprtion measurements

Table S4 Porosity related parameters for all samples derived from N_2-sorption measurements.

	BET surface area[a] (m^2/g)	Total pore volume[b] (cm^3/g)	Main pore width maximum[c] (nm)
			NLDFT
$Cu_{10}Ru$-BTC	603	0.46	0.89
Cu_7Ru-BTC	611	0.47	0.86
Cu_6Ru-BTC	866	0.55	0.89
HKUST-1	1027	0.54	0.92

[a] From N_2-sorption measurements at 77 K (Figure 4a), calculated BET area based on the adsorption points between p/p_0 = 0.01–0.1. [b] Determined based on the adsorption at p/p_0 = 0.9. [c] Calculated by non-local density functional theory (NLDFT) with the model "cylindrical pores at metal oxide".

Matrix-assisted laser-desorption/ionization time-of-flight-mass spectroscopy (MALDI-TOF-MS)

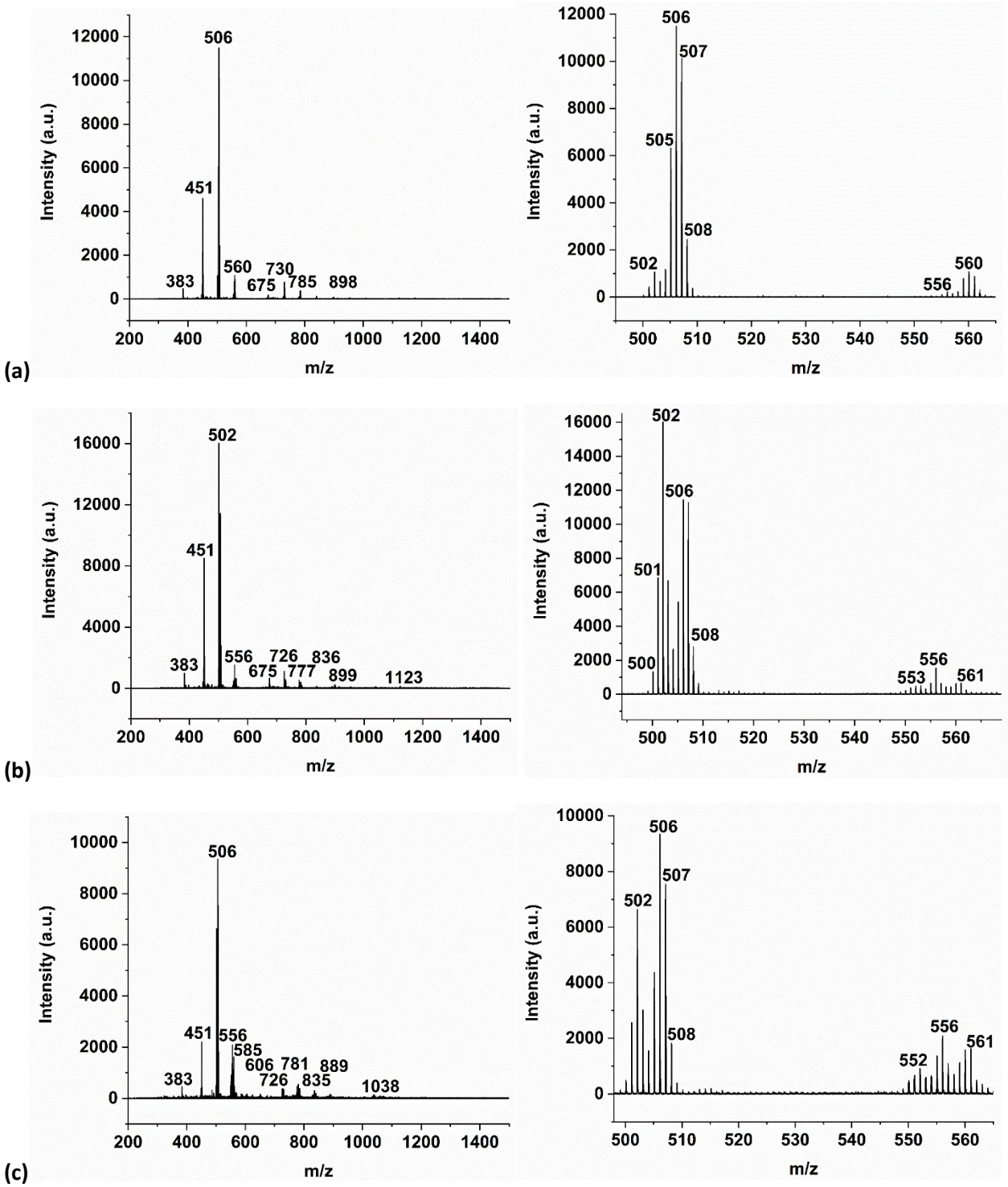

Fig. S14 MALDI-TOF-MS of (a) Cu_6Ru-BTC, (b) Cu_7Ru-BTC and (c) $Cu_{10}Ru$-BTC.

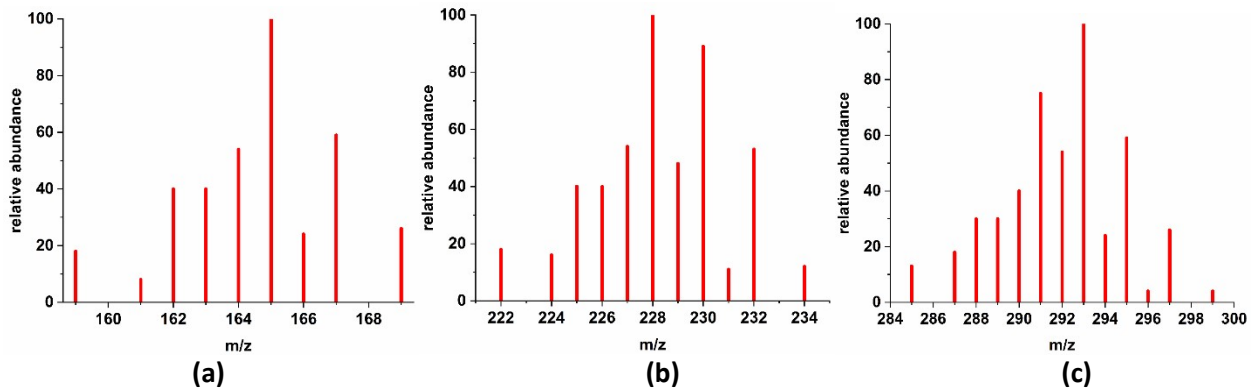

Fig. S15 Calculation of theoretical isotope pattern of (a) CuRu, (b) Cu_2Ru and (c) Cu_3Ru.[2]

X-ray photoelectron spectroscopy (XPS)

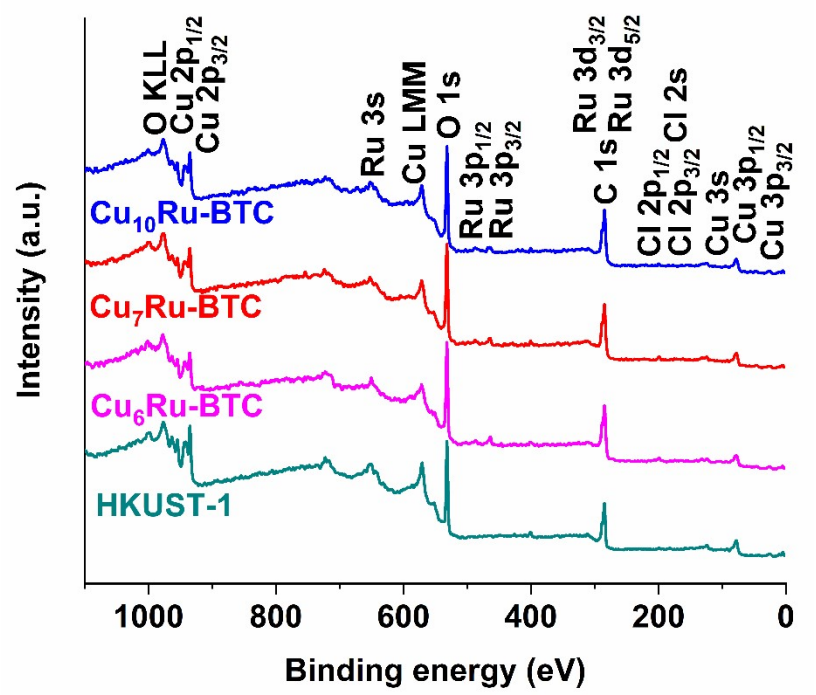

Fig. S16 XPS survey scans for Cu_6Ru-BTC, Cu_7Ru-BTC, Cu_{10}Ru-BTC and mechanochemically synthesized HKUST-1.

High-resolution X-ray photoelectron spectroscopy (HR-XPS)

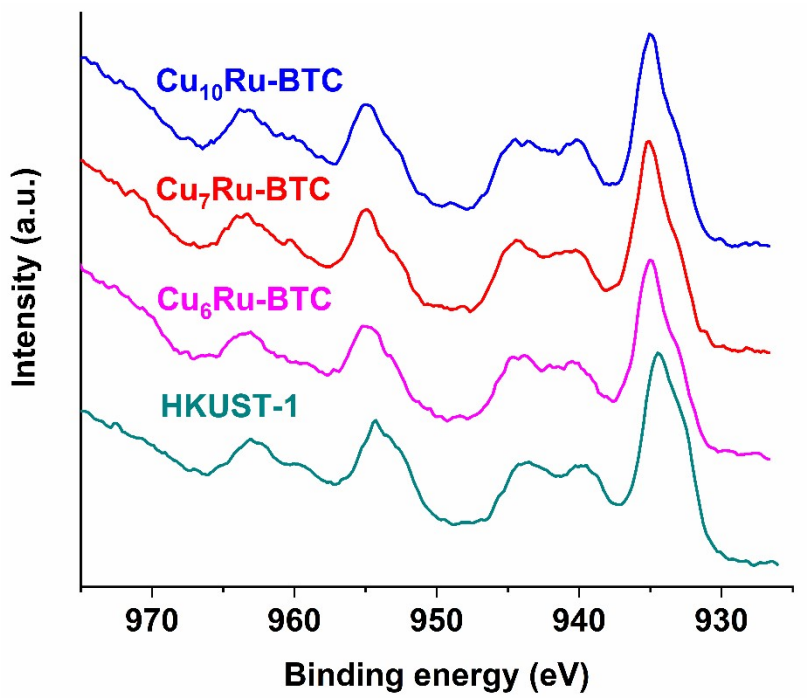

Fig. S17 HR-XPS spectra for the full measurement range of Cu for Cu_6Ru-BTC, Cu_7Ru-BTC, Cu_{10}Ru-BTC and mechanochemically synthesized HKUST-1.

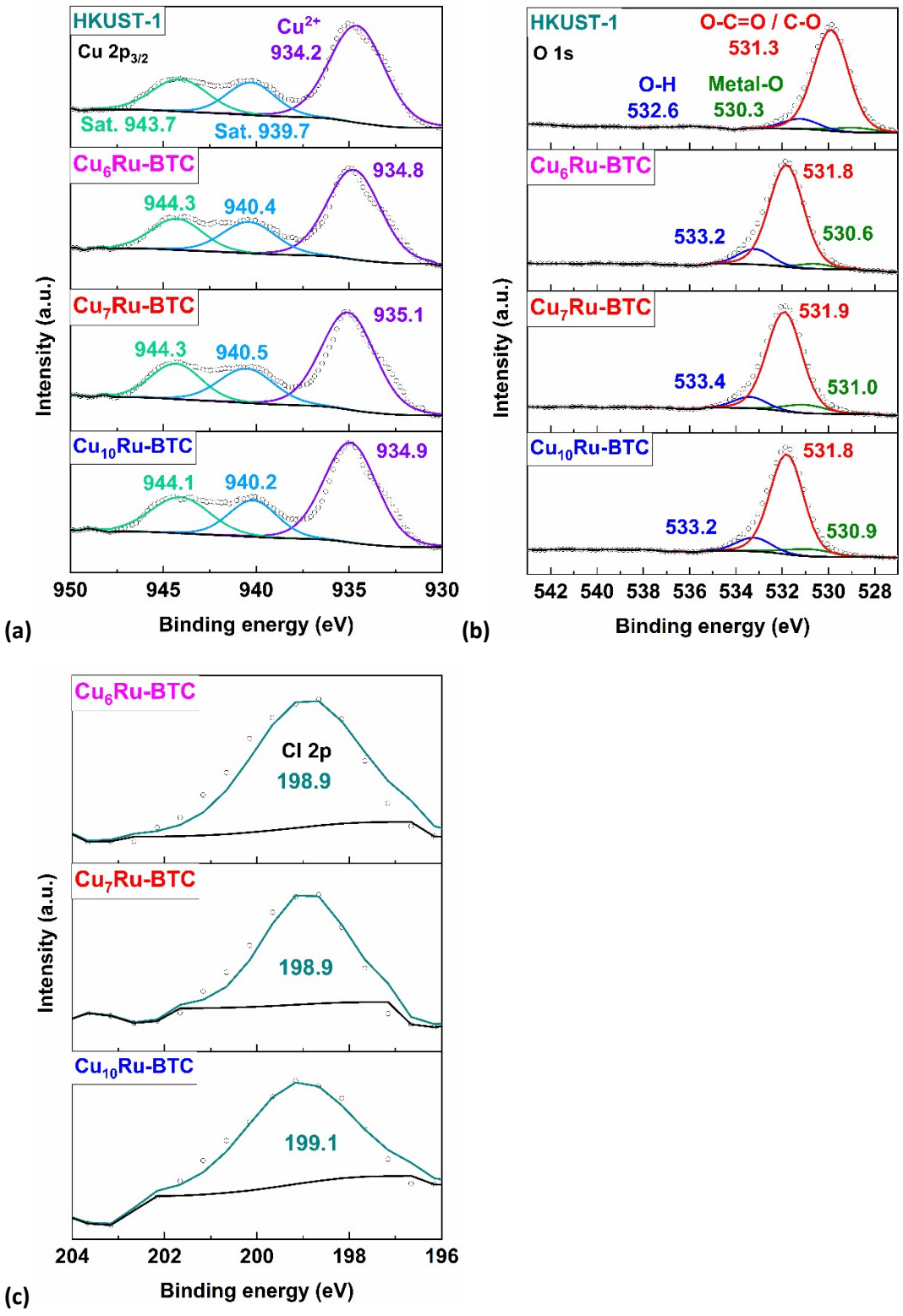

Fig. S18 HR-XPS spectra of (a) Cu $2p_{3/2}$, (b) O 1s and (c) Cl 2p for Cu_6Ru-BTC, Cu_7Ru-BTC, Cu_{10}Ru-BTC and mechanochemically synthesized HKUST-1.

Electrochemical Data

Chronopotentiometry

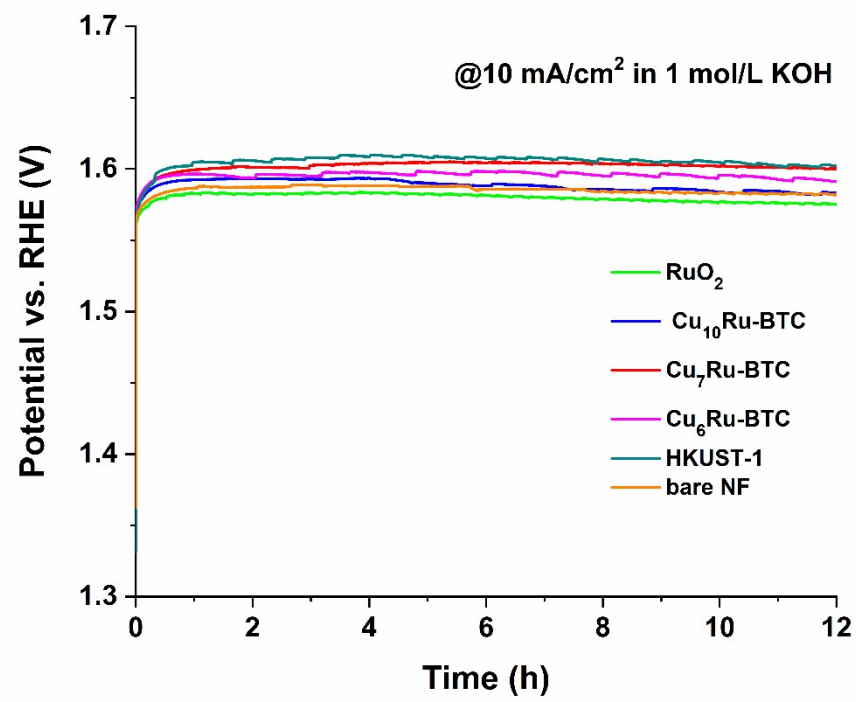

Fig. S19 Chronopotentiometry of Cu_6Ru-BTC, Cu_7Ru-BTC, Cu_{10}Ru-BTC, mechanochemically synthesized HKUST-1, RuO_2 and bare NF for 12 h at a current density of 10 mA/cm^2 in 1 mol/L KOH.

Overpotentials, Tafel slopes and charge-transfer resistances

Table S5 Overpotentials at 10 mA/cm^2 and 50 mA/cm^2, Tafel slope and R_{CT} for all samples tested.

Sample	η @ 10 mA/cm² (mV) before → after 1000 cycles	η @ 50 mA/cm² (mV) before → after 1000 cycles	Tafel slope (mV/dec)	R_{CT} (Ω)
Cu_{10}Ru-BTC	308 → 314	363 → 361	55	13.6
Cu_7Ru-BTC	339 → 319	397 → 364	53	56.1
Cu_6Ru-BTC	376 → 327	436 → 376	63	204.5
HKUST-1	432 → 325	N/A → 372	54	542.4
RuO_2	344 → 312	395 → 357	47	52.8
Bare NF	353 → 316	400 → 360	46	134.2

Electrochemical surface areas (ECSAs)

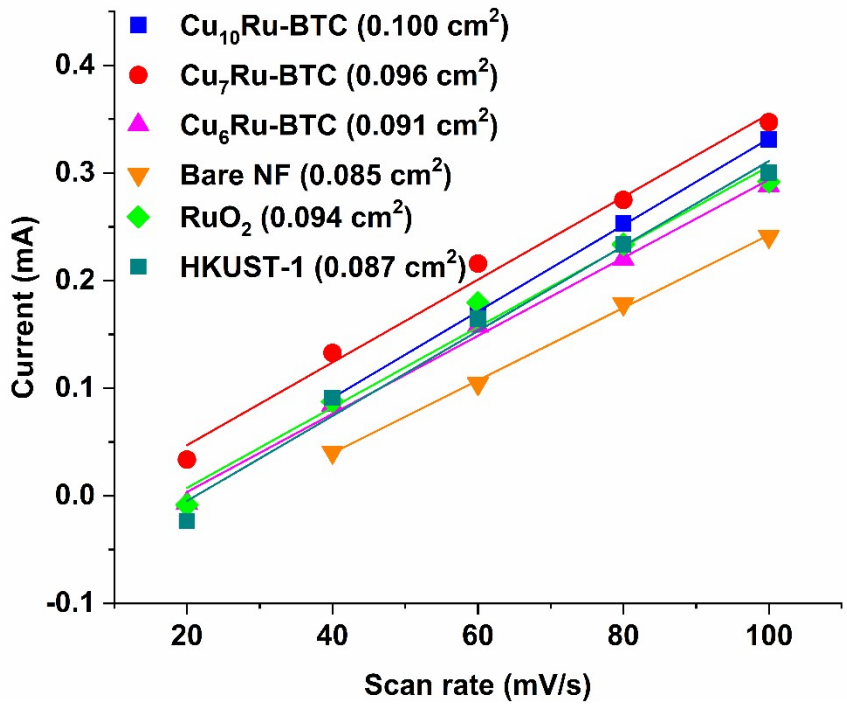

Fig. S20 Scan rate vs. current plot of Cu_6Ru-BTC, Cu_7Ru-BTC, $Cu_{10}Ru$-BTC, mechanochemically synthesized HKUST-1, $RuO_2$and bare NF with their corresponding ECSAs.

Table S6 Double-layer capacitance and ECSA as derived from the current vs. scan rate plot (Fig. S20)

	$Cu_{10}Ru$-BTC	Cu_7Ru-BTC	Cu_6Ru-BTC	HKUST-1	RuO_2	Bare NF
C_{DL} (µF)	4.01	3.85	3.63	3.48	3.74	3.66
ECSA (cm^2)	0.100	0.096	0.091	0.087	0.094	0.085

Faradaic efficiencies (FE)

Table S7 FE without and with correction by the detected percentage of oxygen from a measurement without any applied current to consider the oxygen portion coming from ambient air, which is ascribed to a potential leak in the system.

	$Cu_{10}Ru$-BTC	Cu_7Ru-BTC	Cu_6Ru-BTC	HKUST-1	RuO_2	Bare NF
FE (%) without correction	86	84	82	80	82	77
FE (%) with correction	70	68	66	64	66	61

Physical mixtures of CuO : RuO_2 at different molar ratios

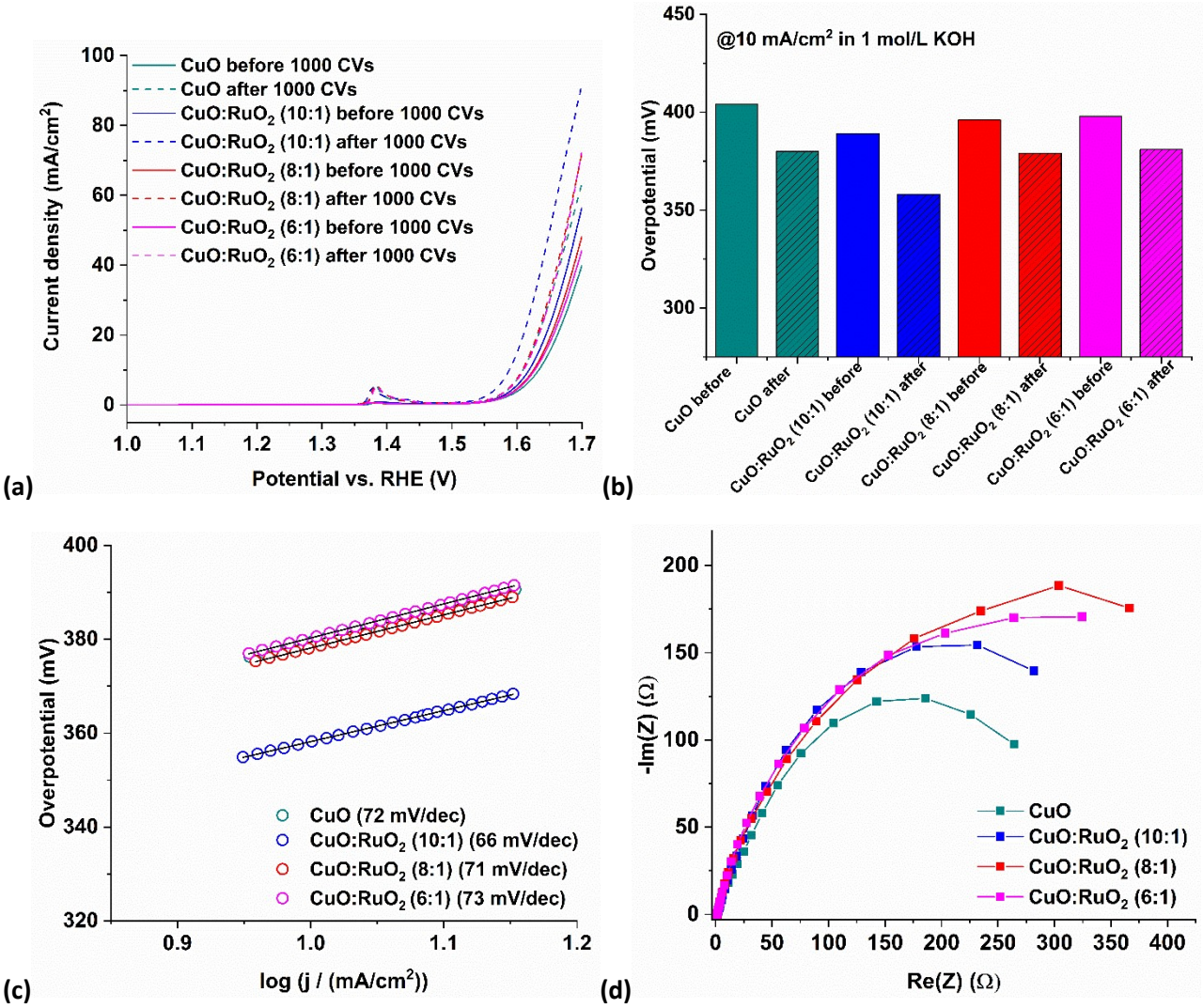

Fig. S21 (a) LSV curves before and after 1000 CVs of CuO and the physical mixtures of CuO:RuO_2 (molar ratio 10:1), CuO:RuO_2 (8:1) and CuO:RuO_2 (6:1) as an ink on nickel foam (NF). (b) Overpotentials calculated from the LSV curves in (a). (c) Tafel plots for CuO and the physical mixtures of CuO:RuO_2 (molar ratio 10:1), CuO:RuO_2 (8:1) and CuO:RuO_2 (6:1). (d) Nyquist plots gathered from EIS for CuO and the physical mixtures of CuO:RuO_2 (molar ratio 10:1), CuO:RuO_2 (8:1) and CuO:RuO_2 (6:1).

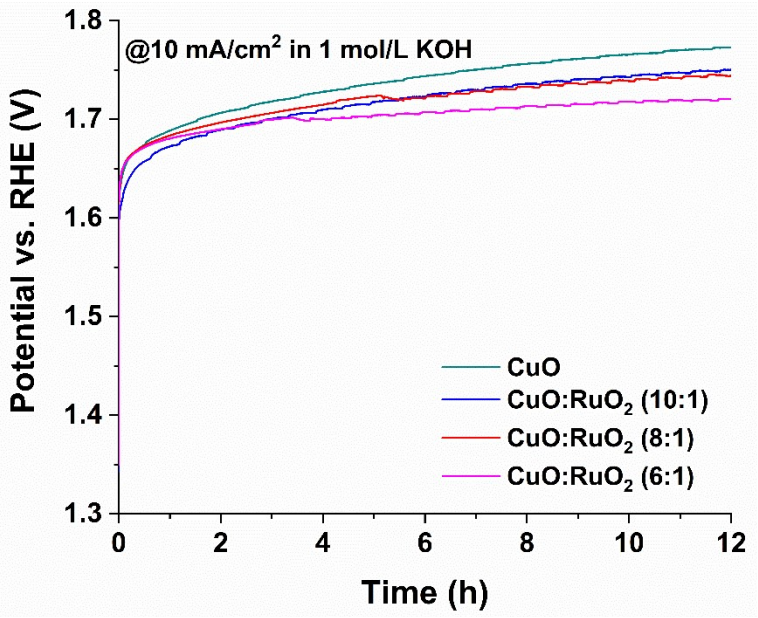

Fig. S22 Chronopotentiometry of CuO and the physical mixtures of $CuO:RuO_2$ (molar ratio 10:1), $CuO:RuO_2$ (8:1) and $CuO:RuO_2$ (6:1) for 12 h at a current density of 10 mA/cm^2 in 1 mol/L KOH.

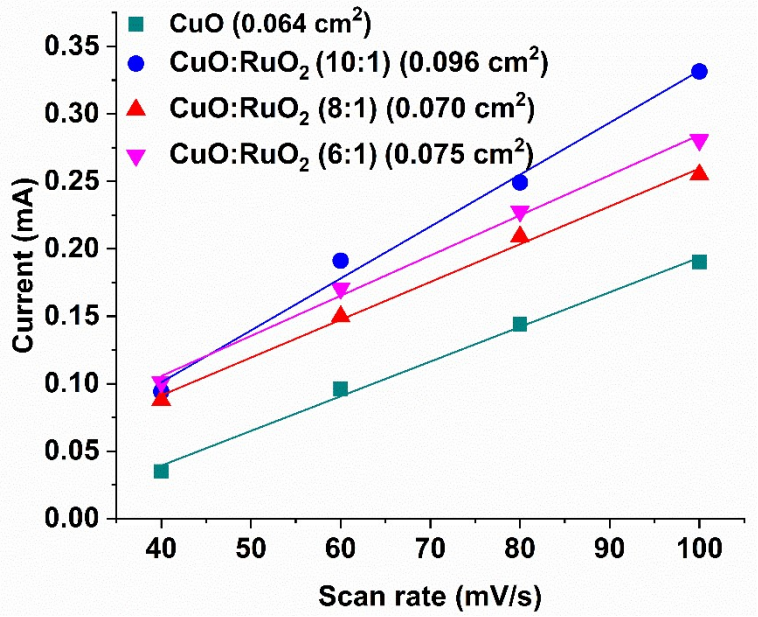

Fig. S23 Current vs. scan rate plot of CuO and the physical mixtures of $CuO:RuO_2$ (molar ratio 10:1), $CuO:RuO_2$ (8:1) and $CuO:RuO_2$ (6:1) with their corresponding electrochemical surface areas, ECSAs.

Table S8 Overpotentials at 10 mA/cm^2 and 50 mA/cm^2, Tafel slope and R_{CT} for CuO and the physical mixtures of CuO:RuO_2 (molar ratio 10:1), CuO:RuO_2 (8:1) and CuO:RuO_2 (6:1).

Sample	η @ 10 mA/cm^2 (mV) before → after 1000 cycles	η @ 50 mA/cm^2 (mV) before → after 1000 cycles	Tafel slope (mV/dec)	R_{CT} (Ω)
CuO	404 → 380	N/A → 451	72	369.5
CuO:RuO_2 (10:1)	389 → 358	462 → 421	66	407.5
CuO:RuO_2 (8:1)	396 → 379	N/A → 445	71	516.2
CuO:RuO_2 (6:1)	398 → 381	N/A → 447	73	470.5

Table S9 Double-layer capacitance and ECSA as derived from the current vs. scan rate plot (Fig. S23†).

	CuO	CuO:RuO_2 (10:1)	CuO:RuO_2 (8:1)	CuO:RuO_2 (6:1)
C_{DL} (μF)	2.57	3.85	2.80	2.98
ECSA (cm^2)	0.064	0.096	0.070	0.075

Post-mortem powder X-ray diffraction (PXRD) of Cu_{10}Ru-BTC and $RuCl_3$ in KOH solution

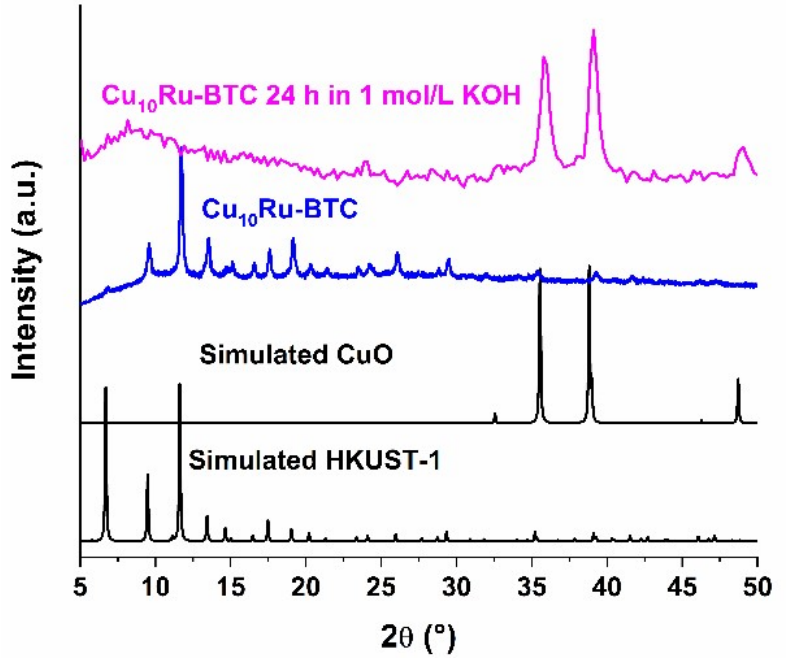

Fig. S24 PXRD patterns of Cu_{10}Ru-BTC following 24 h in 1 mol/L KOH solution, synthesized Cu_{10}Ru-BTC, simulated CuO (COD no. 15-26990) and simulated HKUST-1 (CCDC no. 112954).

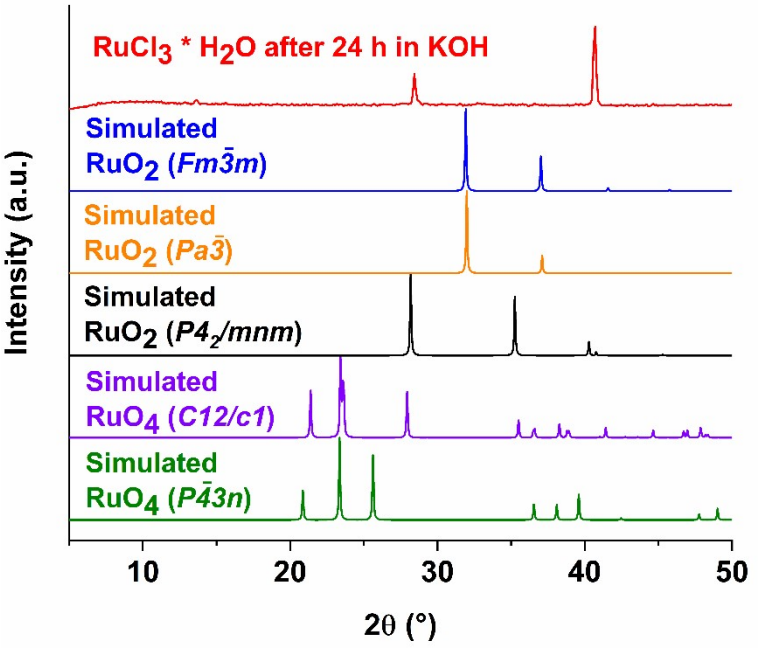

Fig. S25 PXRD patterns of $RuCl_3 \cdot H_2O$ following the immersion for 24 h in 1 mol/L KOH solution and simulated patterns for different polymorphs of RuO_2 (CCDC/ICSD no. 236962, 236965 and 251564) and RuO_4 (CCDC/ICSD no. 415303 and 415306). Then the pattern for tetragonal RuO_2 (space group $P4_2/mnm$) is simulated with preferred orientation along (110) or (010) only the peak at 28° or 40° 2θ, respectively, is seen (March-Dollase parameter 0.1 in both cases). Thus, the experimentally obtained RuO_2 from the KOH treatment of $RuCl_3 \cdot H_2O$ crystallizes predominantly in the (010) preferred orientations and less in the (110) orientation.

Mechanochemical synthesis set-up

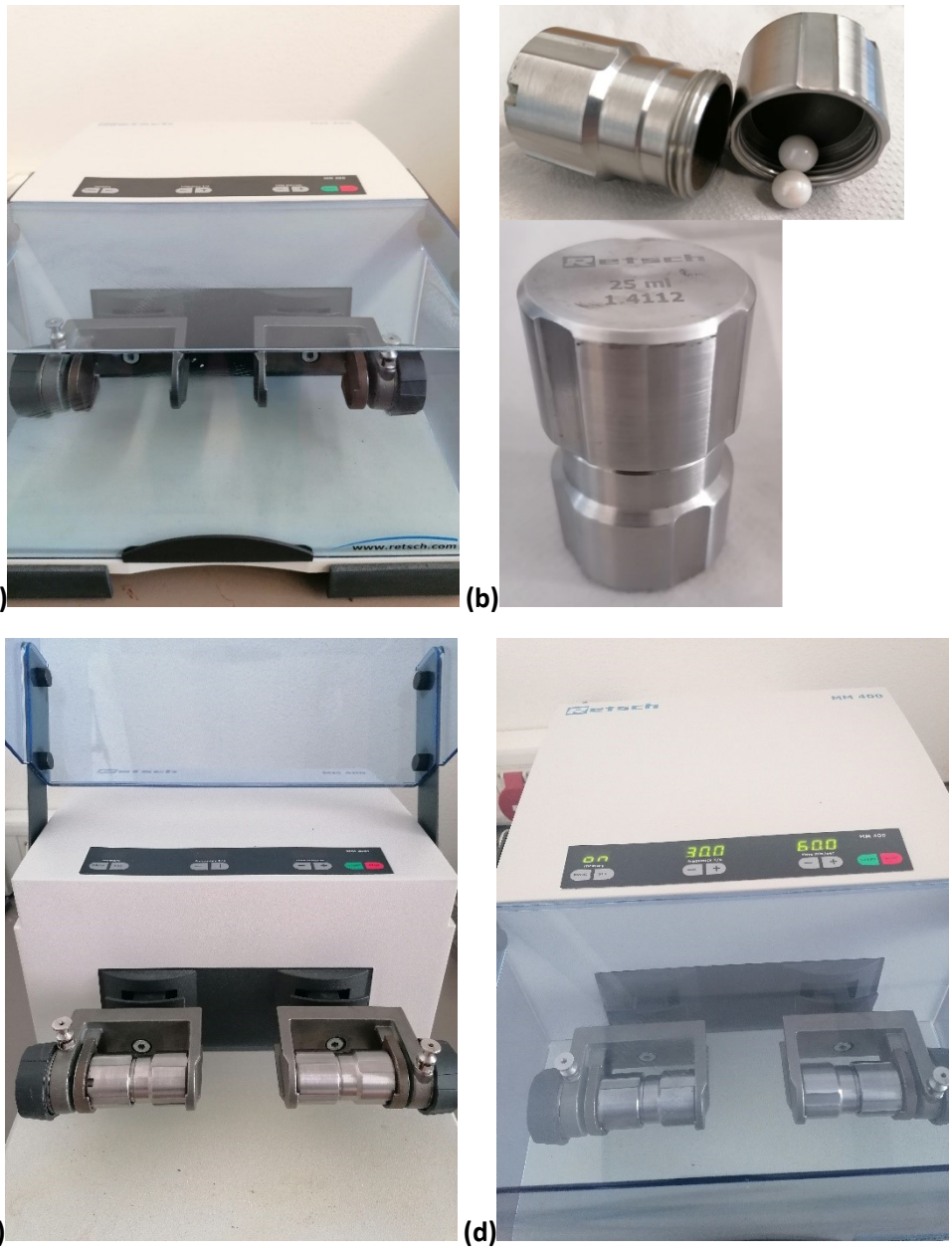

Fig. S26 (a) Retsch MM400 mixer mill without vessels; (b) open and closed 25 mL vessel; (c) Retsch MM400 mixer mill with vessels; (d) Retsch MM400 mixer mill with vessels and input syntheses parameters.

References

1 Y. Chen, X. Mu, E. Lester and T. Wu, *Prog. Nat. Sci.: Mater. Int.,* 2018, **28**, 584-589, DOI: 10.1016/j.pnsc.2018.08.002.

2 M. Loos, C. Gerber, F. Corona, J. Hollender and H. Singer, *Anal. Chem.*, 2015, **87**, 5738-5744, DOI: 10.1021/acs.analchem.5b00941.